Available online at www.sciencedirect.com
ScienceDirect
Magnetic Resonance Imaging 28 (2010) 1165–1174
MAGNETIC RESONANCE IMAGING

Behavioral, electrophysiological and histopathological consequences of systemic manganese administration in MEMRI

Oxana Eschenko[a,*,1], Santiago Canals[a,*,1,2], Irina Simanova[a,3], Nikos K. Logothetis[a,b]

[a]*Max Planck Institute for Biological Cybernetics, 72076 Tübingen, Germany*
[b]*Imaging Science and Biomedical Engineering University of Manchester, M13 9PT Manchester, UK*

Received 6 October 2009; accepted 9 December 2009

Abstract

Manganese (Mn^{2+})-enhanced magnetic resonance imaging (MEMRI) offers the possibility to generate longitudinal maps of brain activity in unrestrained and behaving animals. However, Mn^{2+} is a metabolic toxin and a competitive inhibitor for Ca^{2+}, and therefore, a yet unsolved question in MEMRI studies is whether the concentrations of metal ion used may alter brain physiology. In the present work we have investigated the behavioral, electrophysiological and histopathological consequences of $MnCl_2$ administration at concentrations and dosage protocols regularly used in MEMRI. Three groups of animals were sc injected with saline, 0.1 and 0.5 mmol/kg $MnCl_2$, respectively. In vivo electrophysiological recordings in the hippocampal formation revealed a mild but detectable decrease in both excitatory postsynaptic potentials (EPSP) and population spike (PS) amplitude under the highest $MnCl_2$ dose. The EPSP to PS ratio was preserved at control levels, indicating that neuronal excitability was not affected. Experiments of pair pulse facilitation demonstrated a dose dependent increase in the potentiation of the second pulse, suggesting presynaptic Ca^{2+} competition as the mechanism for the decreased neuronal response. Tetanization of the perforant path induced a long-term potentiation of synaptic transmission that was comparable in all groups, regardless of treatment. Accordingly, the choice accuracy tested on a hippocampal-dependent learning task was not affected. However, the response latency in the same task was largely increased in the group receiving 0.5 mmol/kg of $MnCl_2$. Immunohistological examination of the hippocampus at the end of the experiments revealed no sign of neuronal toxicity or glial reaction. Although we show that MEMRI at 0.1 mmol/Kg $MnCl_2$ may be safely applied to the study of cognitive networks, a detailed assessment of toxicity is strongly recommended for each particular study and Mn^{2+} administration protocol.

Keywords: Manganese; MRI; MEMRI; Toxicity; Behavior; Electrophysiology; Histology; Rat

1. Introduction

The manganese-enhanced magnetic resonance imaging (MEMRI) technique is becoming a powerful tool in systems neuroscience due to its applicability for longitudinal investigations of brain function. For instances, the dynamic behavior of brain networks underlying a wide spectrum of neural processes such as learning, development or neurodegenerative disease can be studied using this technique.

In contrast to other functional magnetic resonance imaging (MRI) modalities [i.e. functional MRI (fMRI) based on the blood oxygenation dependent (BOLD) signal], MEMRI is based on the ability of active neurons to uptake and release a systemically administered MRI reporter, the Mn^{2+} ion [1]. Upon activation, neurons depolarize and Mn^{2+} is taken up through voltage-gated Ca^{2+} channels [2,3]. Although it cannot be applied to humans due to the potential toxicity of the ion (see below), MEMRI has significant advantages, being independent of cerebral blood flow and the nonlinearities of the neurovascular coupling that affect

* Corresponding authors. Oxana Eschenko is to be contacted at Max Planck Institute for Biological Cybernetics, Spemannstrasse 38, Tübingen D-72076, Germany. Tel.: +49 7071 601 1679. Santiago Canals, Instituto de Neurociencias, Campus de San Juan, 03550 San Juan de Alicante, Alicante, Spain. Tel.: +34 965 919202.
E-mail address: scanals@umh.es (S. Canals).
[1] Authors contributed equally.
[2] Dr. S. Canals current address: Instituto de Neurociencias, Campus de San Juan, 03550 San Juan de Alicante, Alicante, Spain.
[3] I. Simanova current address: Max Planck Institute for Psycholinguistics and Donders Institute for Brain, Cognition and Behaviour, Centre for Cognitive Neuroimaging, Nijmegen, The Netherlands.

0730–725X/$ – see front matter © 2010 Elsevier Inc. All rights reserved.
doi:10.1016/j.mri.2009.12.022

conventional fMRI techniques. Mn^{2+} reduces the longitudinal relaxation times (T1), of water protons and consequently, T1-weighted MR images show enhanced signal intensity at the locations where Mn^{2+} ions accumulate, and importantly, proportionally to neuronal activity [4–6]. In combination with appropriate behavioral protocols, MEMRI can be used to visualize specific neural networks that are engaged in a particular cognitive process in awake and behaving animals.

Appropriate protocols are indeed necessary, because manganese is both nutrient and a powerful toxin [7]. The toxic effects of Mn^{2+} overexposure have been known for long time [7,8]. As a consequence, the main problem when applying the MEMRI technique is to keep the equilibrium between the Mn^{2+} doses required for a good MR contrast and signal-to-noise ratio (SNR), and those that are well tolerated by the organism. Excessive accumulation of Mn^{2+} decreases energy metabolism, increases the production of free radicals, and induces cell death of both neurons and glia [9–11]. In a recent report on neuronal tract tracing using MEMRI, we demonstrated that local injections of $MnCl_2$ into the brain parenchyma above 8 nmol results in glial reactivity and above 16 nmol induces massive neuronal cell death [11]. In that work, by controlling Mn^{2+} concentration, pH and osmolarity in the solution we optimized the protocol for intrabrain administration and MEMRI based neuronal tracing. We also introduced the use of implanted micro-osmotic pumps for Mn^{2+} administration and showed the efficiency and low toxicity associated with the slow release of the ion. Detailed investigations of cellular toxicity in MEMRI experiments with systemic Mn^{2+} administration have not yet been reported. However, a plethora of reports in the field of environmental toxicology strongly suggest that some Mn^{2+} dosages used in MEMRI protocols could be affecting the brain and probably heart and lung physiology (for a review see [7,12]). Such toxicity would eliminate any value of Mn^{2+} as an in vivo functional reporter for longitudinal MRI. In addition, as a Ca^{2+} competitor at voltage dependent Ca^{2+} channels, Mn^{2+} may interfere with many intracellular signaling cascades, such as those relevant for synaptic plasticity, memory and learning.

In the present work, we have addressed the issue of Mn^{2+} toxicity by studying the behavioral, electrophysiological and histopathological consequences of systemic manganese administration at concentrations and dosage protocols relevant for MEMRI.

2. Methods

A total of 28 male Sprague-Dawley rats (250–300 g) were used in the present study. Rats were housed in groups of four and had food and water access ad libitum, except for an appetitive learning experiment when rats maintained at approximately 80% of ad libitum weights via restricted food intake (~15–20g per rat/24 h) during the 2-week training period. Rat weight was monitored daily. The 12-h light/dark cycle (8 a.m. lights off) was set in order to perform behavioral training during the dark (most active) phase of the rat circadian rhythm. All experiments were approved by the local authorities (Regierungspraesidium) and were in full compliance with the guidelines of the European community (EUVD 86/609/EEC) for the care and use of the laboratory animals.

2.1. Manganese administration

Manganese was administered acutely in a single sc injection. Isotonic and neutral solutions of $MnCl_2$ were prepared at 20 and 100 mM concentrations for final doses of 0.1 and 0.5 mmol/kg, respectively (equivalent to 16 and 80 mg/Kg of the dehydrated form; $MnCl_2{\cdot}2H_2O$). Manganese solutions were buffered with 10 mM Tris-HCl to a final pH of 7.4 and osmolarity adjusted to 300 mOs/L with NaCl, when required.

2.2. MRI data collection

For the MRI experiments the animals were anesthetized with 1.5–2% isoflurane and placed in a user made saddle coil integrated within a stereotaxic animal holder (RAPID Biomedical, Rimpar, Germany). Temperature, heart rate, CO_2 and SpO_2 were monitored throughout the scanning session. Scans were obtained at different time points after $MnCl_2$ administration (0.5, 1, 4, 12, 24 h). After the last MR session (24 h), animals were let to recover for 1–2 days and then evaluated for electrophysiological parameters.

Experiments were carried out in a vertical 7-T (300 MHz)/60-cm diameter bore magnet (Bruker BioSpin, Ettlingen, Germany). It is equipped with a gradient insert of 38-cm inner diameter (Siemens AC-44; Siemens Medical Solutions, Erlangen, Germany). The gradient system is driven by a Siemens gradient power amplifier with peak voltage of 700 V and current of 500 A. A maximum of 40 mT/m gradient strength per channel can be achieved in less than 150 μs (for more details on the MR system see [13]). The MR system is controlled by a Bruker BioSpec console (ParaVision 3) running under the Linux operating system. We used a modified driven equilibrium Fourier transform (MDEFT) method with MDEFT preparation to obtain T1-weighted anatomical images. The scan parameters were: TR=22.2 ms, TE=4 ms, FA=20°, inversion delay (ID)=1000 ms and four segments. The ID of the MDEFT preparation (responsible for the T1 contrast) was optimized in vivo for the contrast to noise ratio 24 h after MnCl2 administration (data not shown). The geometric parameters of the 3D scans were: matrix 192×112×128, field of view=48×28×32 mm and voxel 0.25×0.25×0.25 mm.

2.3. Electrophysiology

Animals were anesthetized with urethane (1.2–1.5 g/kg, ip) and fastened to a stereotaxic frame. Standard surgical and stereotaxic procedures were applied for the placement of recording and stimulating electrodes, as previously described

[14]. Local anesthetic xylocaine was used additionally for the surgery area. Stainless steel bipolar electrode (WPI, Sarasota, FL, USA) was positioned in the medial perforant path (from lambda: 0 mm anteroposterior and 4.1–4.5 mm lateral, 2.5–3 mm ventral to the dural surface) for orthodromic stimulation of the dentate gyrus (DG) and the hippocampus proper [15]. Recording electrodes were glass micropipettes filled with isotonic $NaCl_2$ (1–1.5 Mμ) and placed at the hilus of the DG (3.5 mm caudal and 2.5 mm lateral, from bregma) guided by the characteristic evoked potentials. A subcutaneous Ag/AgCl wire electrode under the neck skin was used as reference and grounding. The final placement of the stimulating and recording electrodes was adjusted to induce a maximum population spike (PS) in the DG.

For microstimulation of the perforant path, the current amplitude, pulse duration, train duration, and stimulation frequency were controlled digitally by using custom-made software running on the QNX (Canada) real-time operating system. The stimulation pulses were always biphasic and charge-balanced with the cathodal pulse leading the anodal pulse and 0.1 ms in pulse-duration. Test pulses were delivered every 20 s and the evoked potentials elicited by five consecutive pulses were averaged. We generated standard input-output (I/O) curves of the DG by plotting the amplitude of the PS and the slope of the population excitatory postsynaptic potential (EPSP), both derived from the evoked field potential (see Fig. 1C), versus the current intensity applied (0.1 to 1 mA). We generated I/O curves before and after the induction of long-term potentiation (LTP) of synaptic transmission in the hippocampus. LTP was induced by high-frequency stimulation of the perforant path in 3 one-minute episodes separated by 2 minute pauses. Each episode consisted of six trains of four pulses (200 Hz in 40 ms), delivered every 10 s [14]. The current used for LTP induction was the required to generate a PS 50% of its maximal amplitude. Pair pulse facilitation was investigated before LTP by delivering pairs of stimulus at interstimulus intervals ranging from 30 to 200 ms. Facilitation was measured as the percentage increase in the amplitude of the PS elicited by the second vs. the first stimulus.

After band-pass filtering (0.3 Hz–3 kHz) and amplification, the electrophysiological signals were digitalized (22.3 kHz acquisition rate) and stored in a personal computer for offline processing using the Spike2 software (Cambridge Electronic Design, Cambridge, UK). The PS in the hilus of the DG was measured as the amplitude from the precedent positive crest and the negative peak and the EPSP as the maximal slope of the initial raising phase in the recorded potential (Fig. 1 C).

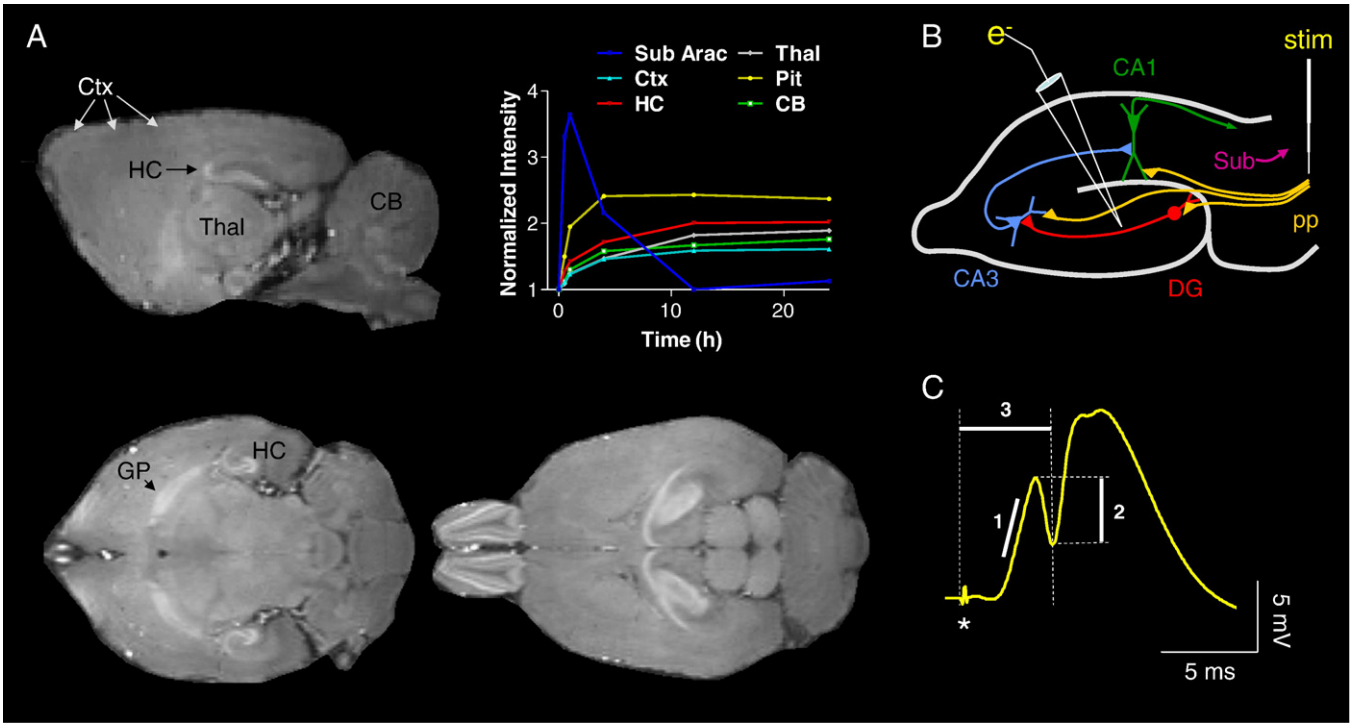

Fig. 1. (A) Representative MEMRI experiment with sc administration of 0.5 mmol/Kg $MnCl_2$. High-resolution T1-weighted anatomical scans demonstrating signal enhancement in the brain were acquired 24h after $MnCl_2$ administration (MDEFT, upper row sagittal view, lower row horizontal views). Time courses of normalized signal intensities in multiple regions of interest are also shown. Note how signal intensity increases in the parenchyma to reach a plateau 24 h after $MnCl_2$ administration. HC, hippocampal formation; Thal, thalamus; CB, cerebellum; GP, globus pallidus; OB, olfactory bulb; Ctx, cortex; Pit, pituitary. (B) Schematic representation of the hippocampal formation illustrating the position of the recording (e-) and stimulating (stim) electrodes used in electrophysiological experiments. pp, perforant path; Sub, subiculum. (C) The population evoked response recorded in the dentate gyrus induced by a single pulse electrical stimulation of the medial perforant path. The slope of EPSP (1) amplitude (2) and latency (3) of the population spike are illustrated.

2.4. Histochemistry

Alter electrophysiological experiments, animals were perfused transcardially after an intraperitoneal lethal dose (~250 mg/kg) of sodium pentobarbital (Narcoren, Merial, Germany) and an injection of 2000 U heparin (Liquemin, Roche Pharma AG, Switzerland) directly into the left ventricle. All blood was rinsed out with 0.9 % warm saline until the outflow from the right atrium was clear (approximately 0.3–0.5 L), followed by 0.1 L of cold paraformaldehyde (PFA; Roti-Histofix 4 %, phosphate-buffered pH 7.0, methanol-stabilized, Carl Roth, Karlsruhe, Germany). The brains were removed from the skulls and were stored in 4% PFA at 4°C overnight. Before sectioning, the whole brains were placed in ascending concentrations of sucrose in 0.1 M phosphate buffer (PB) (10, 20% and 30 %) until they sank; 100-μm-thick coronal frozen sections were then cut serially on a sliding microtome (Microm HM 440E, Walldorf, Germany) and the sections were then either stored at –20°C in cryoprotectant solution (30% ethylene glycol and 10% sucrose in 0.05 M PB) before further processing or immediately stained.

A triple fluorescence histochemical staining was carried out on every third free-floating section and the last remaining series was mounted and stained for Nissl substance. For immunohistochemistry the sections were rinsed three times 5 min each in 0.1 M PB and then incubated for 72 h at 4°C in the blocking solution (10% normal goat serum, self-made by the neighbouring Max Planck Institute (MPI) for developmental biology; 2% bovine serum albumin, Sigma; 0.4 % Triton X-100, Sigma, Schnelldorf, Germany; in 0.1 M. PB) containing the primary antibodies. The primary antibodies used were mouse anti-NeuN (monoclonal anti-neuronal nuclei, IgG1, 2 μg/ml, Chemicon International) and rabbit anti-GFAP (IgG fraction of antiserum, 50 μg/ml, Sigma).

The sections were then washed again 3 times in 0.1 M PBS before they were incubated in the dark another 72 h at 4°C in blocking solution containing the secondary antibodies (Cy3-conjugated goat anti-mouse IgG (H+L), Jackson ImmunoResearch, West Grove, PA, USA, and Alexa Fluor 488 goat anti-rabbit IgG (H+L), Molecular Probes, Invitrogen), each of them diluted by 1:500 to a working concentration of 4 μg/ml. In between two series of three rinses in 0.1 M PB sections were incubated for 5 min in 0.4 ‰ DAPI (4',6-diamidino-2-phenylindole dihydrochloride; Sigma) in dH_20 to label all cell nuclei. Stained sections were mounted on glass slides and cover-slipped with polyvinylalcohol (Mowiol 4-88; Hoechst, Frankfurt, Germany) containing 5% DABCO (1,4-diazobicyclooctane; Merck, Darmstadt, Germany) as an antifading reagent.

Cy3, Alexa Fluor 488 and DAPI images of identical fields of view were acquired using a fluorescence microscope (Axioplan 2, 5x objective; Carl Zeiss, Göttingen, Germany) equipped with appropriate filter sets (AHF, Tübingen, Germany) a CCD camera (Axiocam HRc, controlled by Axiovision 4.5; Zeiss, Göttingen, Germany).

2.5. Behavioral procedures

2.5.1. Apparatus

Rats were tested on a custom-made elevated (84 cm above the floor) T-maze, which was configured from eight-arm radial maze by making three runways accessible from the central platform. The central parts of other five runways were lowered such that 28-cm gap was formed between the edge of the central platform and the distal part of the maze arm. One of the inaccessible maze arms served as an intertrial platform. Black aluminum runways (66×10 cm) extended from a center platform (diameter 30 cm); at the end of each arm a small aluminum cup (diameter 6 cm, depth 1 cm) was located where the reward (chocolate rice cereal, Kellogg's) can be placed. The experimental room was dimly lit. Distinct extra-maze visual cues (e.g., a room door, a window, cabinets, etc.) were present in the room. The experimenter's location was constant relative to the maze, and could thus serve as a cue.

2.5.2. T-maze alternation task

Prior to learning, rats were food-deprived and subjected to a habituation and pre-training procedures during 3–4 days. First, rats were acquainted with reward in their home cages, then they were exposed to an experimental environment with reward randomly distributed all over the maze. The 15-min daily habituation trials were performed until the rats readily moved throughout the maze and consumed the reward. The final preliminary training procedure required rat moving from one end of the maze arm to another and retrieving a single reward placed in the cup on a maze configuration with only two arms accessible.

Next, the rats were trained to perform a T-maze delayed alternation task [16]. Each of ten daily maze tests consisted of two a sample and a choice trials. During the sample trial the two maze arms (start and reward) were available. A rat was placed on the start location at the end of the start arm and was then allowed to visit a single available goal arm and retrieve reward from the cup within 3-min cutoff time. After the rat finished eating, the experimenter placed the rat on the intertrial platform for 30 s delay before the choice trial began. The side of reward location varied randomly across sample trials. The runways were wiped between the sample and choice trials in order to minimize the intramaze cues. During the choice trial, three maze arms (start and two opposite goal arms) were open and the reward was available on the alternative maze arm only. An animal was allowed to correct for an error if it initially went to a nonrewarded arm. After completion of the chosen trial, a rat was placed in the home cage for 3–5 min until the next maze test. If a rat did not reach reward within 3 min either during a sample or choice trials it was placed on the intertrial platform and a new trial would begin after 3–5 min delay. Overall, daily training procedure did not exceed 30 min. Response latency was measured for each trial; for each choice trial, the arm chosen was scored as either correct (alterative to a sample arm) or error (same as a sample arm). The choice accuracy was calculated for each daily session consisting of 10 choice

trials. When rats reached a criterion performance (80% of correct choices for three consecutive days) $MnCl_2$ was injected (sc) 24 h before the behavioral session.

3. Results

3.1. MEMRI

Signal intensity in T1-weighted MR images rapidly increases in the subarachnoidal space and choroid plexus after acute sc injection of Mn^{2+} and peaks 1 h later. Subsequently, very high signal intensity is detected in the pituitary gland (deployed of blood brain barrier) reaching a maximum after approximately 4 h. Finally, Mn^{2+} enhanced signal starts to be detectable in brain parenchyma at 1–2 h after injection and reach a maximum 24 h later. Consistent with the literature [6,17–19], Mn^{2+} distribution in the rat brain after systemic administration is heterogeneous with maximal accumulation at the hippocampus, the globus pallidus and the olfactory bulb. One example of MEMRI and the corresponding time course of normalized signal intensity change after sc injection of 0.5 mmol/Kg of $MnCl_2$ is provided in Fig. 1A.

3.2. Neurophysiology

Due to the avidity of the hippocampus for Mn^{2+} accumulation and the well-known physiology of this brain structure, we performed a series of electrophysiological recordings in the DG to examine possible physiological changes following the Mn^{2+} administration. The basic circuitry of the hippocampal formation has long been well established; the main cortical input is known to arrive from the entorhinal cortex (through the perforant path) and is sequentially channeled to the DG, CA3, CA1, subiculum and back to the entorhinal cortex [20]. In addition, the entorhinal cortex sends direct projections to the hippocampus proper and the subiculum [21]. In our experiments we combined in vivo electric microstimulation of the perforant path with electrophysiological recordings in the DG (see Fig. 1B for a schematic representation) to study possible changes in neural transmission and synaptic plasticity. In specific, we measured the slope of the evoked EPSP that reflects the local population postsynaptic activity, as well as the amplitude and latency of the PS indicating the strength of recruitment of neurons under perforant path stimulation. Finally, we have also applied the standard protocols of pair pulse facilitation (PPF) and LTP in order to investigate changes in presynaptic activity and plasticity that might follow Mn accumulation in hippocampus.

Data in Fig. 2A and B represent the input-output curves recorded in the DG for the EPSP slope and PS amplitude in control and Mn^{2+} treated animals and demonstrate a minor but significant reduction in both parameters for the highest Mn^{2+} concentration [analysis of

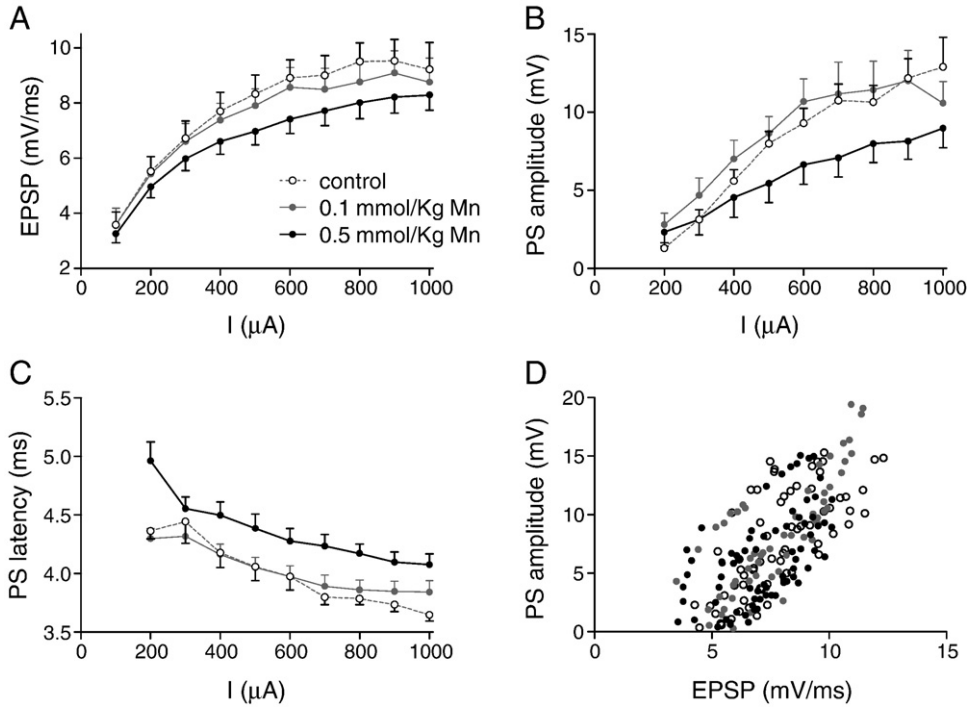

Fig. 2. Effect of a single systemic (sc) injection of two doses of $MnCl_2$ on different measures of the evoked field potential recorded in the dentate gyrus after single pulse electrical stimulation of the perforant path. Maximum slope of EPSP (A), amplitude (B) and latency (C) of the population spike are shown for the intact rats (open circles) and after 0.1 mmol/kg (grey circles) or 0.5 mmol/kg (black circles) of $MnCl_2$. (D) E-S curve illustrating a comparable EPSP to PS ratio between control and $MnCl_2$ treated groups [comparison of slopes by linear regression, $F(2,196)=1.8$, NS].

variance (ANOVA), $F(2,231)=8.4$, $P=.0003$ for EPSP and $F(2,181)=12.5$, $P=.0001$ for PS] with no interaction between treatment and current intensity. Accordingly, the PS latency in the high Mn^{2+} group was increased (Fig. 2C, ANOVA, $F(2,181)=31.0$, $P=.0001$). When the amplitude of individual PS was plotted against their precedent EPSP slopes, instead of the current intensity used to evoke the field potentials (E-S curves), the PS/EPSP ratio was found to be similar for all treatment conditions [Fig. 2D, comparison of slopes by linear regression $F(2,196)=1.8$, $P=.2$]. This result indicates that for a synaptic input of a particular size, the signal propagation, the recruitment of intrinsic currents and the generation of action potentials is not affected by $MnCl_2$. On the basis of this finding, we conclude that tissue excitability is not affected by $MnCl_2$.

The results obtained in the PPF experiments (Fig. 3) demonstrate a dose dependent increase in the facilitation after systemic Mn^{2+} administration [ANOVA, $F(2,72)=14.34$, $P<.001$]. In a PPF protocol, the amplitude of the second PS is increased (facilitated) due to the summation, in the presynaptic terminal, of the actual and residual Ca^{2+} concentrations evoked by the second and first stimulation, respectively. In the presence of a Ca^{2+} competitor, the amplitude of the second PS is proportionally larger than in control conditions. Therefore, the reported increase in PPF under $MnCl_2$ treatment suggests calcium competition at the presynaptic terminal as the mechanism for Mn^{2+} induced reduction of evoked field potentials. Finally, when the ability of synapses to demonstrate a plastic behavior in the presence of Mn^{2+} was tested, no differences were found compared to saline treated animals.

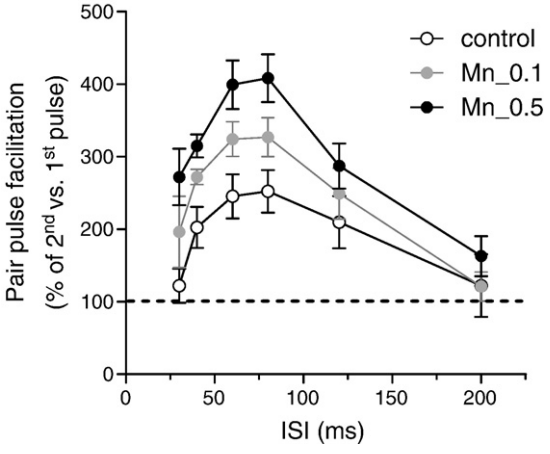

Fig. 3. Effect of a single systemic (sc) injection of two doses of $MnCl_2$ on the PPF of the PS in the hippocampus. The amplitude of the second PS recorded during the activation of the perforant path with pairs of stimulus delivered at interstimulus intervals ranging from 30–200 ms, was dose-dependently decreased by $MnCl_2$ treatment [$F(2,72)=14.34$, $P<.001$]. The result suggest that Mn^{2+} ions competes with Ca^{2+} to enter the presynaptic terminal, interfering with the Ca^{2+}-dependent release of neurotransmitter to the synaptic cleft.

As shown in Fig. 4, the EPSP slope and PS amplitude were largely increased after the tetanization of the perforant path (see Methods for details). The LTP thus obtained was sustained for at least 4h after induction (data not shown). The magnitude of the potentiation was not affected by any of the tested $MnCl_2$ doses (Fig. 4), demonstrating that the LTP of synaptic transmission in the DG is not affected by MEMRI protocols.

3.3. Histopathology

Postmortem immunohistological investigations in the hippocampus, with high degree of Mn^{2+} accumulation, at the end of the electrophysiological or behavioral experiments

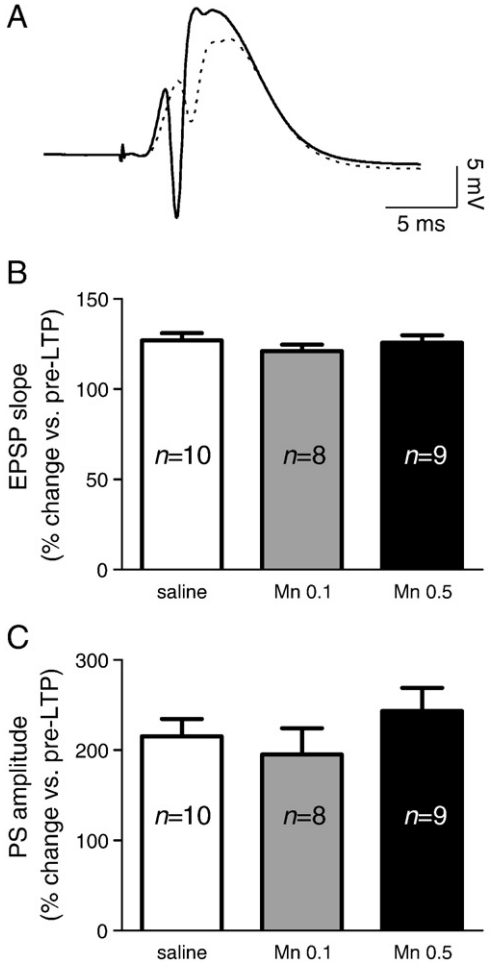

Fig. 4. Effect of a single systemic (sc) injection of two doses of $MnCl_2$ on the LTP in the hippocampus. (A) Representative electrophysiological signals of the evoked field potential recorded in the dentate gyrus before (dashed line) and after (continuous line) the induction of LTP by tetanization of the perforant path. (B) Augmentation of the EPSP slope after LTP in the control group (saline injected, open bar) and the $MnCl_2$ treated animals (0.1 and 0.5 mmol/kg doses, grey and black bars, respectively). (C) Same as (B) but for the PS amplitude. Note that despite the minor but significant reduction on the EPSP slope and PS amplitude with the high $MnCl_2$ dose, the overall degree of synaptic plasticity was comparable between all experimental conditions. Data represent mean±S.E.M.

did not show any sign of gross toxicity (Fig. 5). Neither necrotic nor apoptotic cell death was found by means of cell and nuclei staining under any of the Mn^{2+} treatments. Also, neuronal ($NeuN^{+}$ cells) morphology was preserved and no sign of glial ($GFAP^{+}$ cells) reaction could be found under the studied conditions.

3.4. Behavior

In agreement with the results of hippocampal physiological and histopatholoical examination, the memory performance of the Mn^{2+} treated animals was not affected. Fig. 6 shows the learning of a T-maze delayed alternation task by

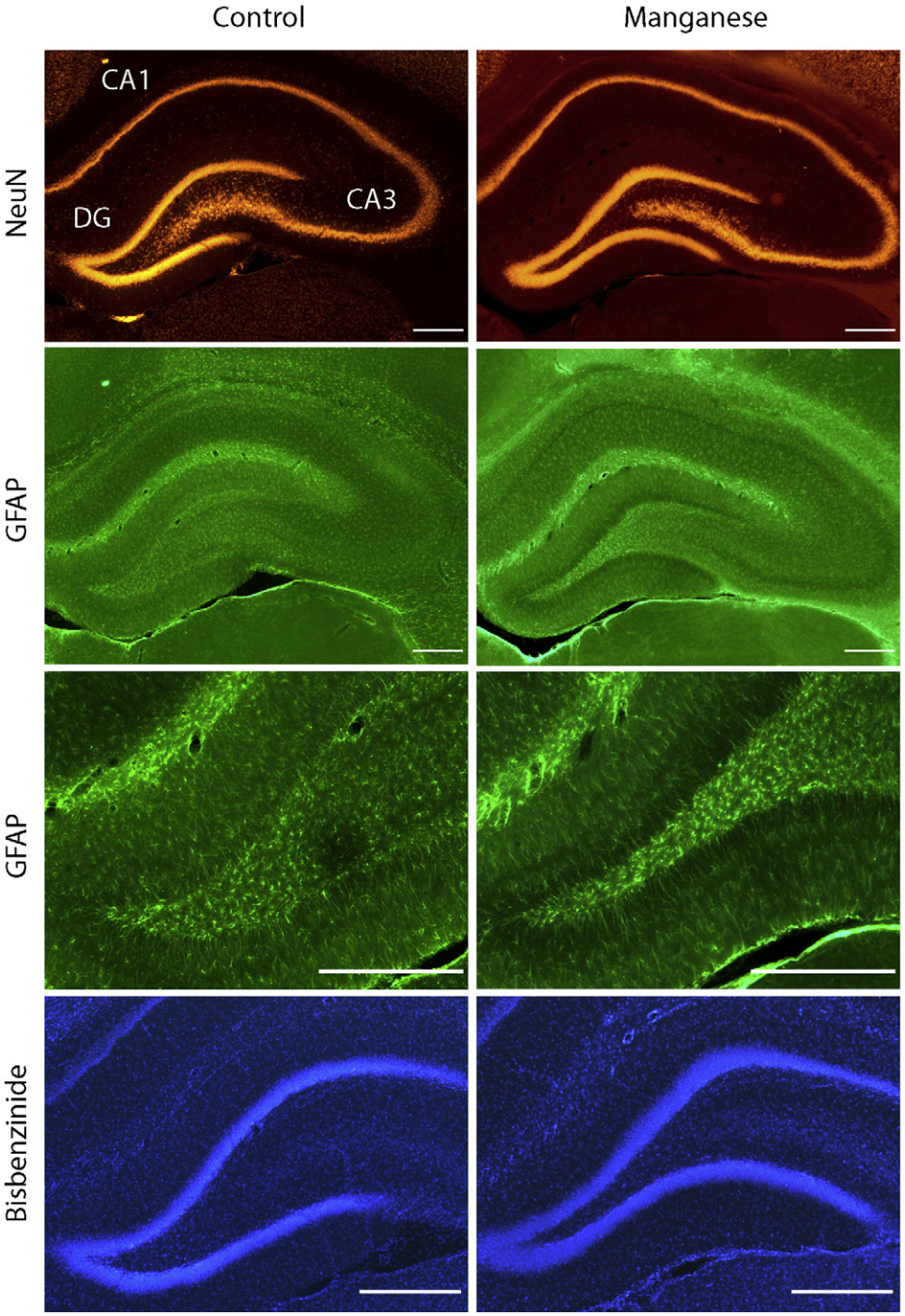

Fig. 5. Immunohistological results obtained in brain sections from control (saline injected) and $MnCl_2$ treated (0.5 mmol/kg) animals. The panels show representative microphotographs at different magnifications of the hippocampus stained with NeuN antibodies (specific for the neuronal population) and glial fibrilary acidic protein (GFAP) antibodies (specific for the astrocyte population) corresponding to control (left panels) or $MnCl_2$ treated animals (right panels). The bisbenzimide staining of cell nuclei is also shown (bottom panels). No difference in the histology were found in any of the investigated animals regardless of the treatment. Calibration bars=0.5 mm.

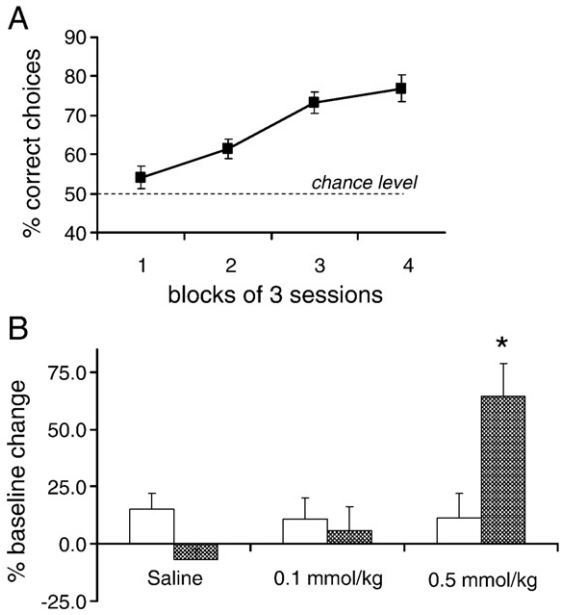

Fig. 6. (A) Learning of a T-maze delayed alternation task by naïve rats (n=12). Mean percentage of correct choices over three consecutive learning sessions is shown. Note, the rats reach an asymptotic performance within 12 sessions. (B) The effect of a single sc injection of saline and two doses of $MnCl_2$ on the task performance 24 h post injection. The percent change for the choice accuracy (open bars) and response latency (dashed bars) is shown. Note, a significant increase of the response latency after injection of a high dose of $MnCl_2$. *P<.05 compared to saline and 0.1 mmol/kg injection.

naïve rats before $MnCl_2$ administration. After reaching the asymptotic performance (12 sessions, see Methods for details) the animals received a single injection of saline or $MnCl_2$ (0.1 or 0.5 mmol/kg) and were retested in the T-maze 24 h later. The choice accuracy in the task was not affected by any Mn^{2+} dose. However, the response latency was increased in Mn-treated rats receiving the highest concentration, likely reflecting the Mn-induced motor disturbances described in toxicology studies [22–25]. Adverse acute side effects of Mn^{2+} on animal general well-being (e.g., drowsiness) may also contributed to the impaired motor performance on the T-maze.

4. Discussion

In the present research, we have investigated the physiological, behavioral and histopathological consequences of systemic Mn^{2+} administration at concentrations and dosage protocols relevant for MEMRI. We found no negative effects after application of a low dose of $MnCl_2$ (0.1 mmol/kg, equivalent to 16 mg/kg of the dihydrated form, $MnCl_2{\cdot}2H_2O$). However, our findings indicate that mild but detectable neurophysiological and behavioral changes can be expected after acute Mn^{2+} administration of higher dosages (0.5 mmol/kg, equivalent to 80 mg/kg $MnCl_2{\cdot}2H_2O$), which are, at present, commonly used for MEMRI.

A single application of $MnCl_2$ at a dose of 0.5 mmol/kg resulted in the decrease of the local population postsynaptic response in the dentate gyrus to perforant path stimulation. This effect is probably the result of Mn^{2+} competition for voltage-gated Ca^{2+} channels at the presynaptic terminal [2,3]. This effect on hippocampal neural transmission did not affect, however, neuronal excitability and did not preclude the expression of long-lasting synaptic plasticity. In well agreement with this result, the behavioral examination demonstrated no effect of Mn^{2+} on the expression of hippocampal-dependent memory as reflected by response accuracy of a previously learned task. However, the response latency was significantly increased after application of the highest dose (0.5 mmol/kg). The later result probably reflects a combination of motor effects of Mn^{2+} accumulation in basal ganglia [24] and side effects on animals general state (e.g., drowsiness) [6,26,27]. In fact, in a recent study we have demonstrated a dose-dependent decrease of rat voluntary running activity after a single application of similar doses of $MnCl_2$ (Eschenko, et al. submitted).

Despite its well-known role as an environmental neurotoxic substance, the concentrations of Mn^{2+} in organism that switch the vital functions of Mn^{2+} into cell toxicity are not well defined. In a similar way, the minimal amount of systemic Mn^{2+} required to produce a detectable contrast change and acceptable SNR needs to be defined (for a particular field strength and scanning protocol). MRI-detectable signal changes at high magnetic field strengths have been reported with doses of $MnCl_2$ around 0.1 mmol/kg (16 mg/kg for $MnCl_2{\cdot}2H_2O$) [18], but more common Mn^{2+} regimes vary between 0.5 and 1 mmol/kg (80–160 mg/kg for $MnCl_2{\cdot}2H_2O$) [6,17,19]. Based on these data and our own results with acute systemic Mn^{2+} administration, the optimal concentration for a particular MEMRI study will most probably be a compromise between acceptable toxic effects and good enough SNR, and therefore, optimal Mn^{2+} concentrations will need to be adjusted for particular applications or experimental questions.

An interesting possibility to increase Mn^{2+} load (and therefore SNR) while keeping the toxicity of the ion to a minimum is the recently introduced use of slow releasing osmotic pumps for Mn^{2+} administration [11] (Eschenko et al., submitted). In our neuronal tract tracing study [11] we demonstrated that Mn^{2+} doses that resulted in dramatic cortical lesions when injected acutely into the brain parenchyma, can be safely applied to the brain when delivered from low concentrated solutions with constant and extremely slow infusion rates. In our recent study we compared the acute behavioral effects of systemic $MnCl_2$ administration via ip or sc injection vs. chronically implanted osmotic pumps. While acute administration resulted in a dose-dependent decrease of rat motor activity, the pump method did not produce any adverse effect (Eschenko et al., submitted). Furthermore, in that study we show that while the pump method was successful in mapping the brain network associated with the running wheel task used, the

acute application of the least toxic dose of $MnCl_2$ (0.1 mmol/kg) failed. These results, together with the findings of the present study indicate that the required doses of $MnCl_2$ for MEMRI-based functional mapping are expected to have physiological and behavioral side effects when acutely applied, and strongly recommend the use of osmotic pumps or similar slow-releasing strategies for functional mapping in behaving animals.

A number of interesting MEMRI studies appeared in the literature mapping brain activity in awake animals [28–30]. In all these studies the authors reported the absence of side effects associated with Mn^{2+} administration even though concentrations of Mn^{2+} in the range of 0.4–0.5 mmol/kg, similar to the highest dosed used in this study, were applied. None of the above mentioned studies, however, performed electrophysiological recordings nor formal behavioral testing requiring, for instances, the movement of the animal in the environment, expression of food motivation, attention, perception or learning abilities. The behavioral task used in the present study requires that the animal actively moves in the maze, remembers the last visited places and makes decisions based on a short-term memory trace. The task permits the differentiation between the motor, motivation and the pure memory components of the behavior. Using this approach, we have shown that Mn^{2+} at all tested concentrations did not interfere with the long-term memory retrieval or the working memory necessary to correctly choose the goal maze arm. However, motor performance was affected by the highest Mn^{2+} dose, increasing the response latency more than 50% with respect to the baseline pre- Mn^{2+} response latency.

The rationale for the selection of the hippocampus as a model-structure to investigate Mn^{2+} toxicity in MEMRI was that Mn^{2+} preferentially accumulates in this area after systemic administration (see Fig. 1), reaching one of the highest concentrations in brain parenchyma (just comparable to those reached in the basal ganglia) and, therefore, a preferential candidate for Mn^{2+} intoxication. However, it must be also noted that high endogenous Fe^{3+} and/or catecholamine levels potentiate the neurotoxicity of Mn^{2+} [31], and therefore, Mn^{2+} accumulation could differentially alter cellular physiology in areas enriched with those substances, like the basal ganglia or the substantia nigra. Indeed, this toxic potentiation is proposed to play a role in human manganism [7] and could also help to explain the motor deficits found in our experiments (Fig. 6B). Additional reasons for choosing the hippocampus as a model system to investigate Mn^{2+} intoxication were the well known electrophysiological properties and synaptic plasticity in the hippocampus in control conditions and the possibility to test its functionality in learning and memory tasks, allowing the investigation of Mn^{2+} toxicity from the cellular physiology up to the behavioral level.

As indicated above, Mn^{2+} intoxication is a well-known cause of Parkinsonism (known as manganism) and dementia. It affects welders, miners, steelworkers and workers in other occupations, who are exposed to manganese fumes. The signs of chronic manganism include disorientation, impairment of memory and judgment, acute anxiety, emotional lability, compulsive acts, hallucinations, illusions and delusions. The underlying mechanisms whereby manganese develops these symptoms are unknown. In this regard, our results offer new information on the neurotoxicity of Mn^{2+}. The rather mild but significant presynaptic effects observed in the hippocampus after a single Mn^{2+} administration may become more relevant after prolonged chronic exposures to the metal ion and explain some of the memory deficits, disorientation, etc. reported in manganism patients. Detailed investigations of T1 relaxation times in the hippocampus of Mn^{2+} exposed humans maybe advisable.

All in all, we consider that the safe application of MEMRI to the study of cognitive networks in freely behaving animals requires a detailed behavioral and neurophysiological investigation of Mn^{2+} toxicity. Special attention must be directed towards the concentration of metal ion applied and its behavioral consequences. Although effects on synaptic plasticity and memory performance were not found significant in the present study for $MnCl_2$ concentrations typically used in MEMRI, the basal synaptic transmission and motor behavior were already affected at the highest Mn^{2+} dose (0.5 mmol/kg). Further improvements on Mn^{2+} administration and MR protocols in order to minimize toxic effects and maximize the SNR of the MR images will further expand the applicability of the technique.

Acknowledgments

We thank Anna L. Keller for the histological processing. This work was supported by the Max Planck Society. S.C. was supported by the Human Frontiers Science Program Organization.

References

[1] Lin YJ, Koretsky AP. Manganese ion enhances T1-weighted MRI during brain activation: an approach to direct imaging of brain function. Magn Reson Med 1997;38:378–88.
[2] Drapeau P, Nachshen DA. Manganese fluxes and manganese-dependent neurotransmitter release in presynaptic nerve endings isolated from rat brain. J Physiol 1984;348:493–510.
[3] Narita K, Kawasaki F, Kita H. Mn and Mg influxes through Ca channels of motor nerve terminals are prevented by verapamil in frogs. Brain Res 1990;510:289–95.
[4] Kang YS, Gore JC. Studies of tissue NMR relaxation enhancement by manganese. Dose and time dependences. Invest Radiol 1984;19:399–407.
[5] Nordhoy W, Anthonsen HW, Bruvold M, Jynge P, Krane J, Brurok H. Manganese ions as intracellular contrast agents: proton relaxation and calcium interactions in rat myocardium. NMR Biomed 2003;16:82–95.
[6] Silva AC, Lee JH, Aoki I, Koretsky AP. Manganese-enhanced magnetic resonance imaging (MEMRI): methodological and practical considerations. NMR Biomed 2004;532:43.
[7] Aschner M, Aschner JL. Manganese neurotoxicity: cellular effects and blood-brain barrier transport. Neurosci Biobehav Rev 1991;15:333–40.
[8] Couper J. On the effects of black oxide of manganese when inhaled into the lungs. Brit Ann Med Pharmacol 1837;41:2.

[9] Hazell AS. Astrocytes and manganese neurotoxicity. Neurochem Int 2002;41:271–7.
[10] Takeda A. Manganese action in brain function. Brain Res Brain Res Rev 2003;41:79–87.
[11] Canals S, Beyerlein M, Keller AL, Murayama Y, Logothetis NK. Magnetic resonance imaging of cortical connectivity in vivo. Neuroimage 2008;40:458–72.
[12] Fitsanakis VA, Zhang N, Avison MJ, Gore JC, Aschner JL, Aschner M. The use of magnetic resonance imaging (MRI) in the study of manganese neurotoxicity. Neurotoxicology 2006;27:798–806.
[13] Pfeuffer J, Merkle H, Beyerlein M, Steudel T, Logothetis NK. Anatomical and functional MR imaging in the macaque monkey using a vertical large-bore 7 Tesla setup. Magn ResonImaging 2004;22: 1343–59.
[14] Canals S, Beyerlein M, Merkle H, Logothetis NK. Functional MRI evidence for LTP-induced neural network reorganization. Curr Biol 2009;398:403.
[15] Paxinos G, Watson C. The rat brain in stereotaxic coordinates. San Diego (CA): Academic Press/Elsevier; 2007.
[16] Deacon RM, Rawlins JN. T-maze alternation in the rodent. Nat Protoc 2006;1:7–12.
[17] Aoki I, Wu YJ, Silva AC, Lynch RM, Koretsky AP. In vivo detection of neuroarchitecture in the rodent brain using manganese-enhanced MRI. Neuroimage 2004;22:1046–59.
[18] Watanabe T, Radulovic J, Spiess J, Natt O, Boretius S, Frahm J. Michaelis T.In vivo 3D MRI staining of the mouse hippocampal system using intracerebral injection of MnCl2. Neuroimage 2004;22: 860–7.
[19] Silva AC, Lee JH, Wu CW, Tucciarone J, Pelled G, Aoki I, et al. Detection of cortical laminar architecture using manganese-enhanced MRI. J Neurosci Methods 2008;167:246–57.
[20] Ramón y Cajal S. Textura del sistema nervioso del hombre y los vertebrados. Berlin: Springer-Verlag; 1998.
[21] Amaral D, Lavenex P. Hippocampal neuroanatomy. In: Andersen P, Morris R, Amaral D, Bliss T, O'Keefe J, editors. The hippocampus book. Oxford: Oxford University Press; 2007. p. 37–114.
[22] Calabresi P, Ammassari-Teule M, Gubellini P, Sancesario G, Morello M, Centonze D, et al. A synaptic mechanism underlying the behavioral abnormalities induced by manganese intoxication. Neurobiol Dis 2001;8:419–32.
[23] Nam J, Kim K. Abnormal motor function and the expression of striatal dopamine D2 receptors in manganese-treated mice. Biol Pharm Bull 2008;31:1894–7.
[24] Newland MC, Weiss B. Persistent effects of manganese on effortful responding and their relationship to manganese accumulation in the primate globus pallidus. Toxicol Appl Pharmacol 1992;113:87–97.
[25] Normandin L, Ann Beaupré L, Salehi F, St.-Pierre A, Kennedy G, Mergler D, et al. Manganese distribution in the brain and neurobehavioral changes following inhalation exposure of rats to three chemical forms of manganese. Neurotoxicology 2005;25:433–41.
[26] Bock NA, Paiva FF, Nascimento GC, Newman JD, Silva AC. Cerebrospinal fluid to brain transport of manganese in a non-human primate revealed by MRI. Brain Res 2008;1198:160–70.
[27] Bock NA, Paiva FF, Silva AC. Fractionated manganese-enhanced MRI. NMR Biomed 2008;221:473–8.
[28] Yu X, Wadghiri YZ, Sanes DH, Turnbull DH. In vivo auditory brain mapping in mice with Mn-enhanced MRI. Nat Neurosci 2005;8:961–8.
[29] Bissig D, Berkowitz BA. Manganese-enhanced MRI of layer-specific activity in the visual cortex from awake and free-moving rats. Neuroimage 2009;44:627–35.
[30] Chuang KH, Lee JH, Silva AC, Belluscio L, Koretsky AP. Manganese enhanced MRI reveals functional circuitry in response to odorant stimuli. Neuroimage 2009;44:363–72.
[31] Sloot WN, van der Sluijs-Gelling AC, Gramsbergen JBP. Selective lesions by manganese and extensive damage by iron after injection into rat striatum or hippocampus. J Neurochem 1994;62:205–16.